



Cite this: *J. Mater. Chem. A*, 2015, **3**, 2634

Lithium-rich $\text{Li}_{1.2}\text{Ni}_{0.13}\text{Co}_{0.13}\text{Mn}_{0.54}\text{O}_2$ oxide coated by Li_3PO_4 and carbon nanocomposite layers as high performance cathode materials for lithium ion batteries[†]

Hui Liu,^a Cheng Chen,^a Chunyu Du,^{*a} Xiaoshu He,^a Geping Yin,^a Bai Song,^b Pengjian Zuo,^a Xinqun Cheng,^a Yulin Ma^a and Yunzhi Gao^a

Lithium-rich layered oxide $\text{Li}_{1.2}\text{Ni}_{0.13}\text{Co}_{0.13}\text{Mn}_{0.54}\text{O}_2$ (LNCMO) coated with a nanocomposite layer of Li_3PO_4 and carbon (LNCMO@ $\text{Li}_3\text{PO}_4/\text{C}$) is designed and facilely prepared as the cathode material for rechargeable lithium ion batteries. The structure and morphology of the LNCMO@ $\text{Li}_3\text{PO}_4/\text{C}$ material are characterized by X-ray diffraction, scanning electron microscopy and transmission electron microscopy, and its electrochemical performance is measured by the constant current charge and discharge, electrochemical impedance spectroscopy and cyclic voltammetry. It is clearly revealed that the LNCMO surface is uniformly coated by the $\text{Li}_3\text{PO}_4/\text{C}$ nanocomposite layer. Moreover, the coating process induces the layer-to-spinel phase transformation, leading to the formation of a spinel nanophasse in the LNCMO@ $\text{Li}_3\text{PO}_4/\text{C}$ material. The presence of $\text{Li}_3\text{PO}_4/\text{C}$ composite coating with high ionic and electronic conductivity and the spinel nanophasse synergistically contribute to the electrochemical properties. Therefore, the LNCMO@ $\text{Li}_3\text{PO}_4/\text{C}$ material shows a high discharge capacity of $124.4 \text{ mA h g}^{-1}$ even at a current density of 1000 mA g^{-1} , a remarkable capacity retention of 87.3% after 200 cycles, and a desirable initial coulombic efficiency of 87.0%. The LNCMO@ $\text{Li}_3\text{PO}_4/\text{C}$ material represents an attractive alternative to high-rate and long-life electrode materials for lithium-ion batteries.

Received 15th September 2014
Accepted 3rd December 2014

DOI: 10.1039/c4ta04823g
www.rsc.org/MaterialsA

Introduction

Along with the rapid development of portable electronic devices, electric/hybrid electric vehicles and stationary energy storage, the demand for lithium-ion batteries (LIBs) with high energy density has promoted enormous research efforts to develop cathode materials,^{1,2} which act as the source of lithium ions and dominate the energy density of LIBs.³ Conventional layered metal oxide materials, such as LiCoO_2 and $\text{LiNi}_{1/3}\text{Co}_{1/3}\text{Mn}_{1/3}\text{O}_2$, and olivine metal phosphate materials, such as LiFePO_4 and LiMnPO_4 , have low specific capacity and cannot satisfactorily meet the requirement for the high energy density of LIBs.⁴ In recent years, Li-rich layered oxides with a composition of $x\text{Li}_2\text{MnO}_3 \cdot (1-x)\text{LiMO}_2$ ($0 < x < 1$, M = Ni, Co, Mn) have attracted a substantial amount of attention as promising cathode materials,^{5–11} because they are able to deliver a reversible discharge capacity of $>250 \text{ mA h g}^{-1}$ when charged above 4.6 V, lower the cost and improve the safety of LIBs.¹² However,

these Li-rich layered oxides exhibit poor cycling stability due to the unstable electrode/electrolyte interface at high voltages and irreversible phase transition during cycling.^{13–16} Moreover, their rate capability is undesirable, because the Li_2MnO_3 component has a low Li^+ diffusion coefficient and electronic conductivity.^{17,18} In addition, the irreversible electrochemical activation of the Li_2MnO_3 component involves oxygen and Li^+ extraction, which leads to the low initial coulombic efficiency.¹⁹

In order to address these problems, several strategies have been proposed, including bulk doping, acid leaching, surface coating and composite designing. Among them, surface coating has been proved to be an effective strategy,^{20–28} because the surface modification layers hinder the direct contact and the side reactions between the electrode and the organic electrolyte, and thus effectively improve the cycling stability of the Li-rich layered oxides. Unfortunately, most of the surface modification materials, commonly including the oxides, phosphates and fluorides, are poor ionic and/or electronic conductors, which are harmful to the rate performance and even reversible capacity of the Li-rich layered oxides. Therefore, the ideal surface modification layers have to be highly Li^+ and electron conductive, which will enhance the cycling stability and rate performance of Li-rich layered oxides simultaneously.

^aSchool of Chemical Engineering and Technology, Harbin Institute of Technology, Harbin, 150001, China. E-mail: cydu@hit.edu.cn

^bHarbin Coslight Power Co., Ltd., No. 8 Taihu South Street, Harbin, 150060, China

† Electronic supplementary information (ESI) available. See DOI: 10.1039/c4ta04823g

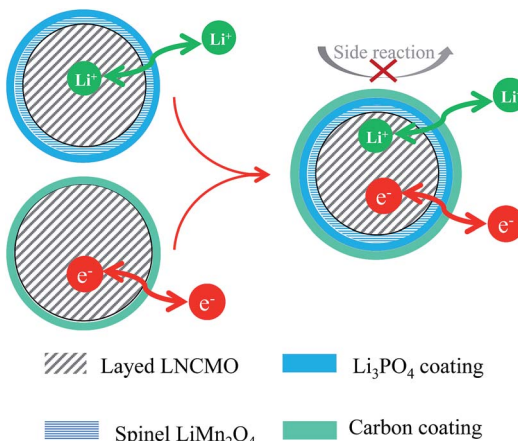


Fig. 1 Design of $\text{Li}_{1.2}\text{Ni}_{0.13}\text{Co}_{0.13}\text{Mn}_{0.54}\text{O}_2$ coated by a $\text{Li}_3\text{PO}_4/\text{C}$ nanocomposite layer with high ionic and electronic conductivity as well as stable interface.

Li_3PO_4 with high Li^+ diffusion coefficient has been widely used to coat and improve the rate performance of LiFePO_4 , LiCoO_2 , LiMnPO_4 , $\text{Li}(\text{Ni}_{0.4}\text{Co}_{0.3}\text{Mn}_{0.3})\text{O}_2$, and $\text{Li}_2\text{FeSiO}_4$ materials.^{29–36} Carbon is also an effective coating material to improve the electronic conductivity and stabilize the electrode/electrolyte interface for the cathode active materials,³⁷ such as LiFePO_4 ,^{38–40} LiMn_2O_4 ,⁴¹ and $\text{LiNi}_{1/3}\text{Co}_{1/3}\text{Mn}_{1/3}\text{O}_2$.⁴² In this article, we prepared the spherical Li-rich layered oxide, $\text{Li}_{1.2}\text{Ni}_{0.13}\text{Co}_{0.13}\text{Mn}_{0.54}\text{O}_2$ (LNCMO), *via* a coprecipitation process followed by a high temperature reaction. The nanocomposite layer of Li_3PO_4 and carbon ($\text{Li}_3\text{PO}_4/\text{C}$) was then coated on the LNCMO material by facile solid state processes, which is of low-cost and is easy to reproduce. The $\text{Li}_3\text{PO}_4/\text{C}$ nanocomposite coating layer not only has high ionic and electronic conductivity, but also is able to stabilize the interface and reduce the side reaction between the cathode and the electrolyte (Fig. 1). Meanwhile, the coating process induces the transformation from the layer to the spinel phase. Therefore, the resulting $\text{Li}_3\text{PO}_4/\text{C}$ coated LNCMO (LNCMO@ $\text{Li}_3\text{PO}_4/\text{C}$) material exhibits improved rate capability and cyclability. Moreover, the coulombic efficiency of the LNCMO@ $\text{Li}_3\text{PO}_4/\text{C}$ material is significantly enhanced. Thus, this LNCMO@ $\text{Li}_3\text{PO}_4/\text{C}$ material is a promising high performance cathode material for LIBs.

Experimental

Preparation of materials

A pristine lithium-rich layered $\text{Li}_{1.2}\text{Ni}_{0.13}\text{Co}_{0.13}\text{Mn}_{0.54}\text{O}_2$ (LNCMO) material was synthesized by a high temperature solid state reaction from LiOH and $\text{Ni}_{0.167}\text{Co}_{0.167}\text{Mn}_{0.666}\text{CO}_3$ precursor. The $\text{Ni}_{0.167}\text{Co}_{0.167}\text{Mn}_{0.666}\text{CO}_3$ precursor was prepared by a co-precipitation method. In brief, 2 mol L^{-1} aqueous solution of NiSO_4 , CoSO_4 and MnSO_4 (1 : 1 : 4 in molar ratio) and 2 mol L^{-1} aqueous solution of Na_2CO_3 with a desirable amount of NH_4OH were separately pumped into a continuously stirred tank reactor for 12 h under a nitrogen atmosphere at 60 °C. During the precipitation process, the

pH of the mixed solution was kept at 7.5. The precipitated $\text{Ni}_{0.167}\text{Co}_{0.167}\text{Mn}_{0.666}\text{CO}_3$ precursor was filtered, washed with deionized water, and then dried in a vacuum at 110 °C. The obtained $\text{Ni}_{0.167}\text{Co}_{0.167}\text{Mn}_{0.666}\text{CO}_3$ powder was thoroughly mixed with an appropriate amount of $\text{LiOH}\cdot\text{H}_2\text{O}$ (3 mol% excess) and calcined at 900 °C for 20 h in air to gain a pristine layered lithium-rich LNCMO material. To prepare the LNCMO@ $\text{Li}_3\text{PO}_4/\text{C}$ material, the Li_3PO_4 coated LNCMO (LNCMO@ Li_3PO_4) material was first synthesized by thoroughly mixing the pristine LNCMO material with $\text{NH}_4\text{H}_2\text{PO}_4$ in a mole ratio of 20 : 1 and sintering at 450 °C for 5 h in air. 0.2 g of Super P was then dispersed in *N*-methyl pyrrolidone, into which 2.0 g of LNCMO@ Li_3PO_4 was added. This mixture was then ultrasonicated for 2 h and dried in a vacuum at 110 °C. Finally, the dried powder was fired at 350 °C for 2 h and cooled down to room temperature to obtain the LNCMO@ $\text{Li}_3\text{PO}_4/\text{C}$ material.

Physical characterization

The crystalline phase of synthesized products was characterized using a Panalytical Empyrean powder X-ray diffractometer using $\text{Cu K}\alpha$ radiation. The X-ray diffraction (XRD) pattern was analyzed by the Rietveld refinement method using General Structure Analysis System (GSAS) software. The morphology and structure of the samples were observed using a FEI QUANTA 200 FEG field emission scanning electron microscope operating at 20 kV and a Tecnai G2F30 high resolution transmission electron microscope equipped with an energy dispersive X-ray (EDX) analyzer operating at 300 kV. The Li_3PO_4 and carbon contents in the LNCMO@ $\text{Li}_3\text{PO}_4/\text{C}$ sample were determined by X-ray fluorescence (XRF) using a Panalytical AXIOS-PW4400 spectrometer and an Epigraphy JS-DN328 carbon–sulfur analyser, respectively. The Brunauer–Emmett–Teller (BET) surface area was measured with a BeiShiDe 3H-2000PS1 instrument after the samples were vacuum dried at 200 °C for 4 h.

Electrochemical testing

Electrochemical testing was performed using CR2025-type coin cells with Li metal foil as the counter electrode, which were assembled in an argon filled glove box. For fabrication of the cathodes, the active materials (LNCMO, LNCMO@ Li_3PO_4 and LNCMO@ $\text{Li}_3\text{PO}_4/\text{C}$) were thoroughly mixed with Super-P conductive carbon black and a poly(vinylidene fluoride) binder (80 : 10 : 10 in weight) in *N*-methyl pyrrolidone. The obtained slurry was coated onto Al foil, and dried overnight at 120 °C in a vacuum. The electrolyte solution was 1.0 M LiPF_6 in a mixture of ethylene carbonate and dimethyl carbonate (1 : 3 in volume). Charge and discharge behaviors of the cells were tested using a constant current method. Electrochemical impedance spectroscopy (EIS) was recorded with an electrochemical workstation PARSTAT 2273 over a frequency range of 10 mHz to 100 kHz. Cyclic voltammogram curves were measured using a CH Instrument 604D electrochemical workstation in a potential range of 2.0 V to 4.6 V at a scan rate of 0.1 mV s^{-1} .

Results and discussion

Synthesis of LNCMO@Li₃PO₄/C materials

The crystalline structures of the LNCMO, LNCMO@Li₃PO₄ and LNCMO@Li₃PO₄/C materials are revealed by powder X-ray diffraction (XRD) as shown in Fig. 2A. Most reflections in the pattern of the LNCMO material can be indexed to the layered α -NaFeO₂ structure. A few weak short-ranged superlattice reflection peaks appear between 20° and 25°, corresponding to the ordering of the Li⁺ and Mn⁴⁺ ions in the Li₂MnO₃ structure.¹⁹ This XRD pattern is consistent with the previous reports,⁴³ indicating that the LNCMO material has been successfully synthesized. In comparison, the LNCMO@Li₃PO₄ and LNCMO@Li₃PO₄/C materials exhibit reflections corresponding to Li₃PO₄ at 22.3°, 23.2°, 24.8° and 34.7°, and the cubic spinel structure at 36.4°, 38.1°, 44.1° and 68.1°, which are clearly observed by the magnified XRD patterns (Fig. 2B), in addition to those of the layered α -NaFeO₂ structure. The presence of Li₃PO₄ and spinel phase can be explained by the reaction of NH₄H₂PO₄ and Li₂MnO₃ at high temperature. During the reaction, NH₄H₂PO₄ induces partial chemical leaching of Li from

Li₂MnO₃ to form Li₃PO₄ coating on the surface, leaving some Li_{2-x}MnO₃ components. Simultaneously, the high temperature (450 °C) promotes the migration of Mn to the empty Li sites and Li to the Mn sites in the Li_{2-x}MnO₃ components, leading to the layer-to-spinel phase transformation. As a result, the LNCMO@Li₃PO₄ material contains some spinel oxides and Li₃PO₄. A similar reaction mechanism has been proved by Sun *et al.* and our group.^{23,43} It is noteworthy that, after carbon coating, the crystalline structure of the LNCMO@Li₃PO₄/C material does not change obviously, suggesting that carbon coating is a mild process. The carbon content in the LNCMO@Li₃PO₄/C material is measured to be 2.25% using a carbon and sulfur analyser, revealing that carbon has been coated on the surface. The Li₃PO₄ content in the LNCMO@Li₃PO₄/C sample is determined to be 3.12% by the Rietveld refinement within the *R*³*m* phase and *Pmn21* phase (Fig. S1†), which is roughly consistent with the XRF result (3.68%).

The morphology of the LNCMO, LNCMO@Li₃PO₄ and LNCMO@Li₃PO₄/C materials is examined by scanning electron microscopy (SEM). Fig. 3 shows SEM images of the three materials for various magnifications. The pristine LNCMO material (Fig. 3A1–A3) consist of nanoporous spherical agglomerates with the particle size varying from 10 to 15 μ m, whose surface is rather smooth and clear. This well-organized micro-nano-structure is expected to facilitate electrolyte penetration into the particles, thus providing more interface area between the electrode material and the electrolyte.⁴⁴ After the surface modification (Fig. 3B1–C3), the spherical shape and particle size of the LNCMO material are maintained, indicating that the modification processes do not significantly damage the morphology of the LNCMO material. From the magnified SEM images (Fig. 3B3 and C3), however, it can be noted that the surface of the LNCMO@Li₃PO₄ and LNCMO@Li₃PO₄/C materials becomes rough, and some small nanoparticles and

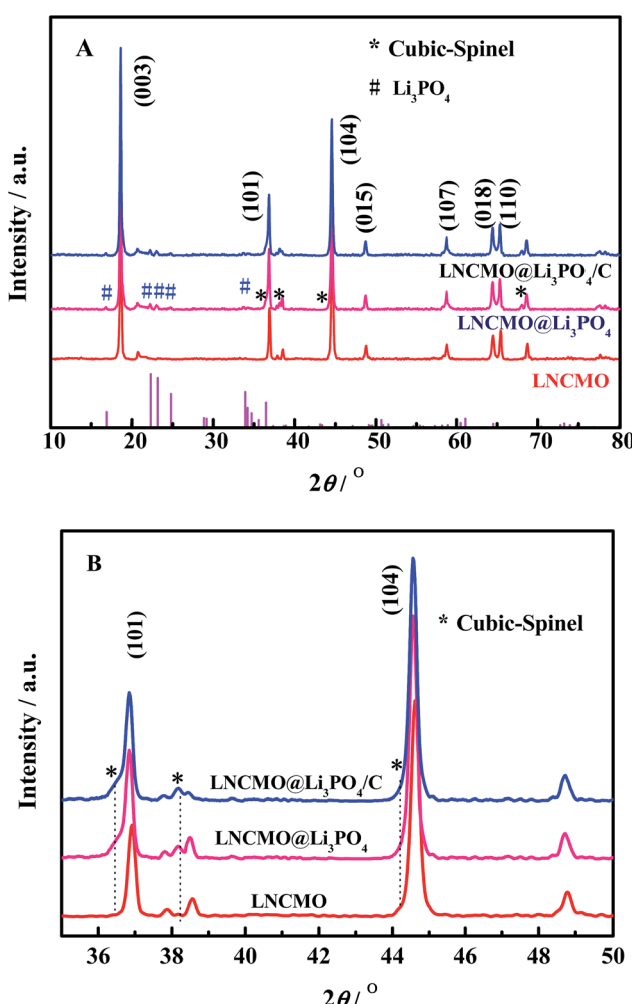


Fig. 2 Powder XRD patterns of the LNCMO (A1–A3), LNCMO@Li₃PO₄ (B1–B3) and LNCMO@Li₃PO₄/C (C1–C3) materials in a 2θ range of 10–80° (A) and 35–50° (B).

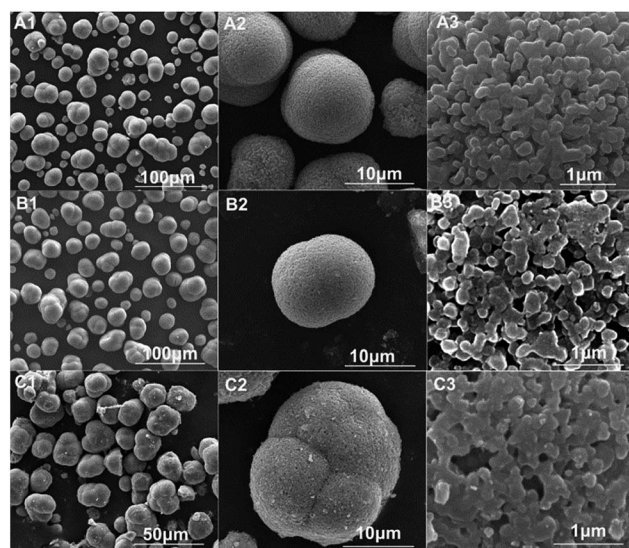


Fig. 3 SEM images of LNCMO (A1–A3), LNCMO@Li₃PO₄ (B1–B3) and LNCMO@Li₃PO₄/C (C1–C3) materials.

indistinct layers are observed on the surface of the materials, especially for the LNCMO@Li₃PO₄/C material, which suggests that the surface of the LNCMO material might be successfully coated by Li₃PO₄ and carbon.

The composition and structure of the LNCMO, LNCMO@Li₃PO₄ and LNCMO@Li₃PO₄/C materials are characterized by transmission electron microscopy (TEM), and the results are given in Fig. 4. From the high-resolution TEM (HRTEM) image of the LNCMO material (Fig. 4A), the interlayer spacing is measured to be 0.47 nm and 0.24 nm, corresponding to the (003) and (101) fringes of the layered structure, respectively. Moreover, these fringes are rather straight and no

interruption is visible, revealing a perfect crystalline layered structure. From the HRTEM image of the LNCMO@Li₃PO₄ material (Fig. 4B), however, the interplanar spacing of the lattice fringes is measured to be 0.47 nm and 0.29 nm, which is well indexed to the (111) and (220) planes of cubic spinel structures, respectively. Moreover, there seems a thin layer with a thickness of 1 ~ 2 nm covering on the material surface (indicated by an arrow). These findings confirm the transformation from layered to spinel phases and formation of Li₃PO₄ coating during the reaction between NH₄H₂PO₄ and LNCMO. From the HRTEM images of the LNCMO@Li₃PO₄/C material (Fig. 4C–F), it is observed that the material interior still maintains the layered structure, while there are some spinel nanograins (marked by ellipses in Fig. 4C) decorated within the exterior, indicating that the solid phase reaction between NH₄H₂PO₄ and LNCMO takes place on the surface of the LNCMO material and induces a small amount of layered to spinel phase transformation. The selected area electron diffraction on the surface of the LNCMO@Li₃PO₄/C material confirms the presence of both layered and spinel phases (Fig. 4G and H). In addition, there is a layer with a thickness of 2 ~ 5 nm covering on the material surface (Fig. 4C), which is thicker than that for the LNCMO@Li₃PO₄ material, confirming that carbon has been coated on the surface. The chemical composition of the coating layer in the LNCMO@Li₃PO₄/C material is examined using EDX elemental mapping (Fig. S2†), which exhibits uniform distribution of P and C elements in the coating layer, suggesting the uniform Li₃PO₄ and carbon coating. The BET surface area of LNCMO, LNCMO@Li₃PO₄ and LNCMO@Li₃PO₄/C materials is measured to be 1.96 m² g⁻¹, 2.85 m² g⁻¹ and 5.02 m² g⁻¹, respectively, which further verifies the nanostructure of the coating layers. The nanocomposite coating layer of Li₃PO₄ and carbon on the surface of the LNCMO material will have high ionic and electronic conductivity and protect the LNCMO material from electrolyte attack, leading to improved electrochemical performance.

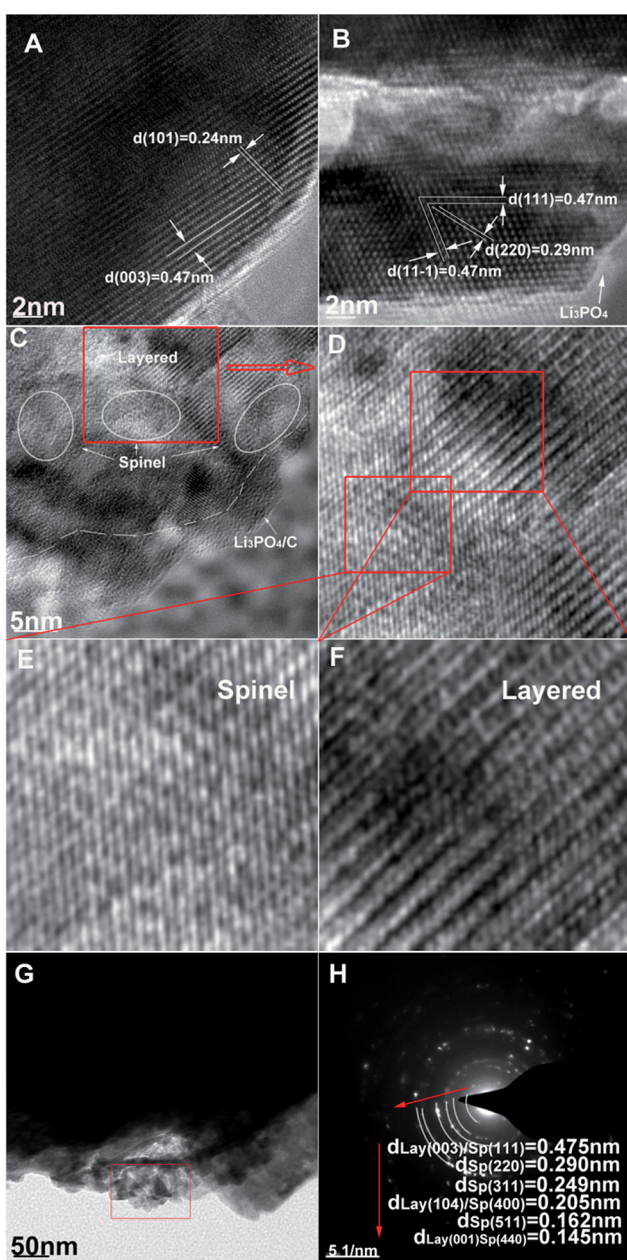


Fig. 4 HRTEM images of the LNCMO (A), LNCMO@Li₃PO₄ (B) and LNCMO@Li₃PO₄/C (C–F) materials, and TEM image (G) and electron diffraction pattern (H) of the LNCMO@Li₃PO₄/C material.

Electrochemical performance

Fig. 5 compares the initial charge/discharge curves and corresponding differential capacity (dQ/dV^{-1}) profiles for the LNCMO, LNCMO@Li₃PO₄ and LNCMO@Li₃PO₄/C electrodes between 2.0 V and 4.6 V at a current density of 30 mA g⁻¹ (0.1 C). From the charge/discharge curves (Fig. 5A), the LNCMO electrode exhibits a discharge capacity of 266.2 mA h g⁻¹ with a coulombic efficiency of 83.3%, meaning a large irreversible capacity loss of 53.1 mA h g⁻¹, which is caused by the irreversible activation of Li₂MnO₃.¹² In comparison with the pristine LNCMO electrode, the LNCMO@Li₃PO₄ electrode shows a higher coulombic efficiency (87.0%) and lower irreversible capacity loss (37.5 mA h g⁻¹). This should be ascribed to the spinel structure transformed from Li₂MnO₃ during the reaction between NH₄H₂PO₄ and LNCMO, because the charge voltage plateau around 4.5 V becomes short, which is related to the concomitant extraction of lithium and oxygen from Li₂MnO₃, and the discharge voltage plateau around 2.8 V gets longer, which is the characteristic of the spinel structure. Further, the

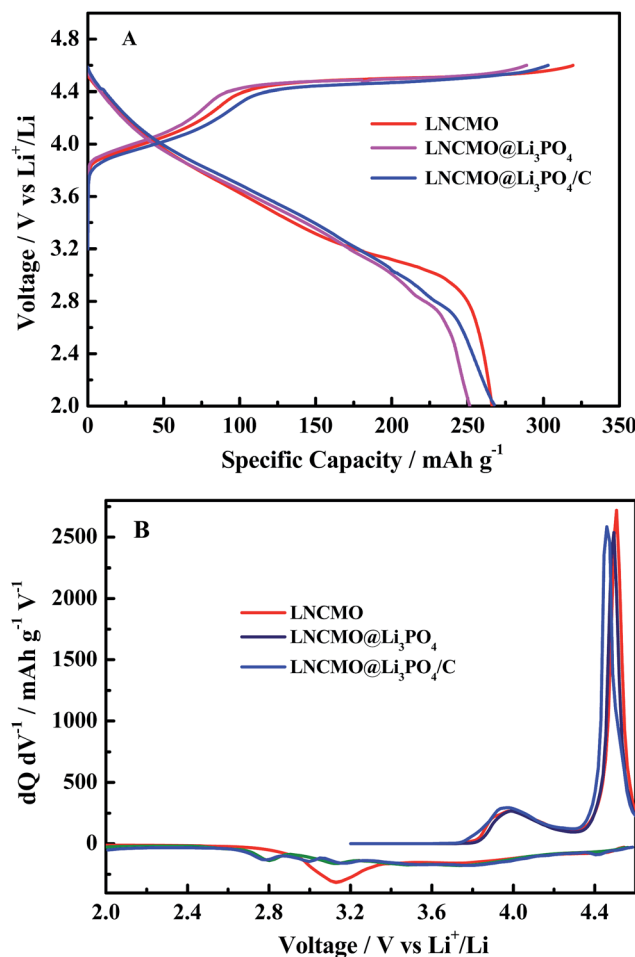


Fig. 5 Initial charge/discharge curves (A) and corresponding differential capacity ($dQ\text{ }dV^{-1}$) profiles (B) of the LNCMO, LNCMO@Li₃PO₄ and LNCMO@Li₃PO₄/C electrodes at a current density of 30 mA g^{-1} .

LNCMO@Li₃PO₄/C electrode presents an even higher initial coulombic efficiency of 88.3% and lower charge/discharge polarization than the LNCMO@Li₃PO₄ and LNCMO electrodes, which suggest that the nanocomposite coatings of Li₃PO₄ and carbon improve the Li insertion/desertion performance of the LNCMO material. From the differential capacity profiles (Fig. 5B), lower charge/discharge polarization and emergence of the voltage plateau around 2.8 V can be clearly distinguished for the LNCMO@Li₃PO₄/C electrode, confirming the positive contributions of the nanocomposite coating of Li₃PO₄ and carbon to the electrochemical performance.⁴⁵

The rate performance of the LNCMO, LNCMO@Li₃PO₄ and LNCMO@Li₃PO₄/C electrodes is shown in Fig. 6A. Over the whole range of current density tested, the LNCMO@Li₃PO₄/C electrode presents higher rate performance than the LNCMO and LNCMO@Li₃PO₄ electrodes. At a current density of 1000 mA g^{-1} , the reversible capacity of the LNCMO and LNCMO@Li₃PO₄ electrodes is 72.5 mA h g^{-1} and 98.5 mA h g^{-1} , corresponding to 27.2% and 38.6% of the capacity at a current density of 30 mA g^{-1} , respectively. In contrast, the capacity of the LNCMO@Li₃PO₄/C electrode remains at 124.4 mA h g^{-1} at the same current density, corresponding to 46.7% of its capacity

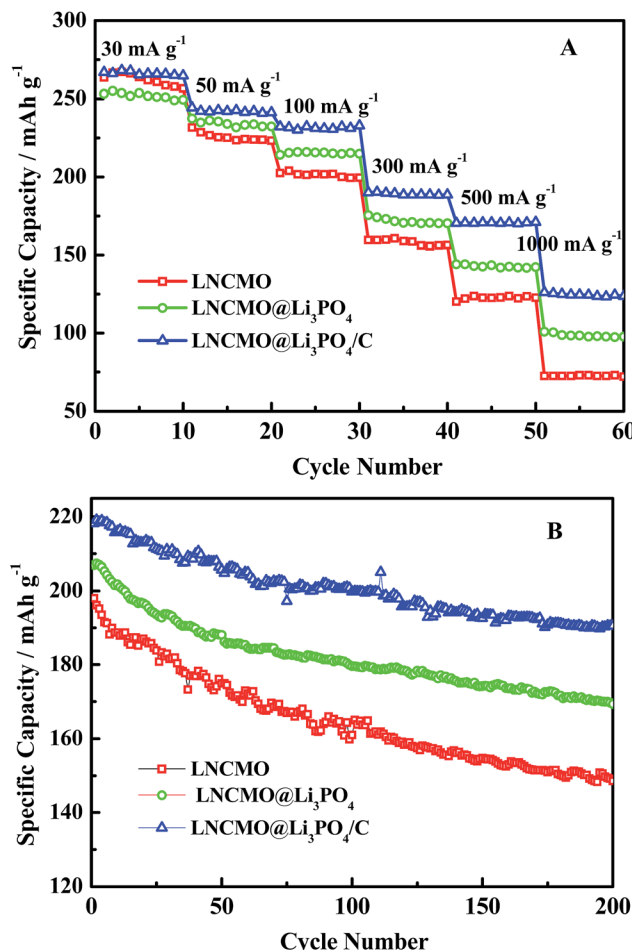


Fig. 6 Rate capability (A) and cycling performance at a current density of 150 mA g^{-1} (B) for the LNCMO, LNCMO@Li₃PO₄ and LNCMO@Li₃PO₄/C electrodes between 2.0 V and 4.6 V.

at a current density of 30 mA g^{-1} , which is over 71% higher than that of the LNCMO electrode. The outstanding rate performance of the LNCMO@Li₃PO₄/C electrode is in line with our expectation and mainly results from its unique Li₃PO₄/C nanocomposite coating layer, which has high Li⁺ and electron conductivity simultaneously as revealed previously.⁴⁵ In addition, the spinel phase on the exterior of the material also contributes positively to the rate performance because it has been reported that the spinel phase has a fast Li⁺ diffusion coefficient.²³

Fig. 6B shows the cycling stability of the LNCMO, LNCMO@Li₃PO₄ and LNCMO@Li₃PO₄/C electrodes between 2.0 V and 4.6 V at a current density of 150 mA g^{-1} . The LNCMO@Li₃PO₄ and LNCMO@Li₃PO₄/C electrodes exhibit both higher capacity and better cycling stability than the pristine LNCMO electrode. After 200 cycles, the LNCMO electrode delivers a capacity of 198.0 mA h g^{-1} with a capacity retention of 75.1%. However, the LNCMO@Li₃PO₄ and LNCMO@Li₃PO₄/C electrodes yield a capacity of 207.0 mA h g^{-1} and 218.3 mA h g^{-1} after the same cycles, corresponding to a capacity retention of 82.0% and 87.3%, respectively. We believe that the enhanced cycling performance of the LNCMO@Li₃PO₄/C electrode can be

attributed to the following facts: (1) the $\text{Li}_3\text{PO}_4/\text{C}$ nanocomposite coating layer effectively inhibits side reactions between the electrode and the organic electrolyte, and (2) the spinel phase has higher structural stability than the layered structure.³³

In order to further understand the superior electrochemical performance of the LNCMO@ $\text{Li}_3\text{PO}_4/\text{C}$ electrode, the electrochemical impedance spectroscopy (EIS) plots of the LNCMO, LNCMO@ Li_3PO_4 and LNCMO@ $\text{Li}_3\text{PO}_4/\text{C}$ electrodes in the charged state of 4.3 V at the first and fiftieth cycles are given in Fig. 7A1–C1. Each EIS plot exhibits a high-frequency semicircle, an intermediate-frequency semicircle and a low-frequency tail, which is ascribed to the solid electrolyte interface (SEI) resistance, the charge transfer resistance of the electrode/electrolyte interface, and the Li^+ ion diffusion process in the solid phase of the electrode, respectively.⁴⁶ At the first cycle, both SEI resistance and charge transfer resistance of the LNCMO@ $\text{Li}_3\text{PO}_4/\text{C}$ electrode are significantly lower than those of the LNCMO electrode, and even the LNCMO@ Li_3PO_4 electrode, confirming that the nanocomposite coating of Li_3PO_4 and carbon facilitates the Li^+ and electron transfer, which are mainly responsible for the high rate capability of the LNCMO@ $\text{Li}_3\text{PO}_4/\text{C}$ material. After 50 cycles, the impedance of the LNCMO electrode is increased to over 400 Ω from around 200 Ω . Such a considerable increase in the impedance reveals that the capacity fading of the LNCMO electrode may be attributed to the formation of undesired side reaction products that impede the electrochemical reaction during cycling.⁴⁷ In comparison, the impedance growth is suppressed for the LNCMO@ Li_3PO_4 electrode, suggesting that the Li_3PO_4 coating layer prevents the direct exposure of LNCMO to

the electrolyte during cycling. Moreover, the impedance variation for the LNCMO@ $\text{Li}_3\text{PO}_4/\text{C}$ electrode is even smaller, which is consistent with its cyclability and means that carbon coating also has a positive impact on the cycling performance.

More evidence of the positive contribution of the $\text{Li}_3\text{PO}_4/\text{C}$ nanocomposite coating on the electrochemical performance of the LNCMO material is illustrated by cyclic voltammetry (CV) at the first and fiftieth cycles (Fig. 7A2–C2). In these CVs, the first pair of oxidation/reduction (O1/R1) peaks slightly below 4.0 V is predominantly associated with the oxidation and reduction of Ni and Co ions in the $\text{LiNi}_{0.33}\text{Co}_{0.33}\text{Mn}_{0.33}\text{O}_2$ component, whereas the second pair of oxidation/reduction (O2/R2) peaks below 3.5 V is probably attributed to the redox reaction of Mn ions in the activated MnO_2 derived from the Li_2MnO_3 component.^{12,17} It is noteworthy that a weak oxidation peak appears around 3.0 V for LNCMO@ Li_3PO_4 and LNCMO@ $\text{Li}_3\text{PO}_4/\text{C}$ electrodes (indicated by arrows), which is related to the presence of the spinel phase,⁴⁸ confirming the transformation from layered to spinel phases during the coating process. At the first cycle, the oxidation peak of Mn ions for the LNCMO@ Li_3PO_4 and LNCMO@ $\text{Li}_3\text{PO}_4/\text{C}$ electrodes is invisible, which is consistent with the presence of the spinel phase, suggesting that the spinel phase is probably beneficial to stabilizing the Li_2MnO_3 component and the activation of Li_2MnO_3 takes place gradually from the exterior to the interior. After 50 cycles, the reduction peak of Mn ions shifts negatively by 0.1 V, whereas the oxidation peak of Ni and Co ions shifts positively by 0.13 V for the LNCMO electrode, which suggest that the substantial side reactions happen and the electrochemical polarization is greatly increased during cycling. In contrast, no significant

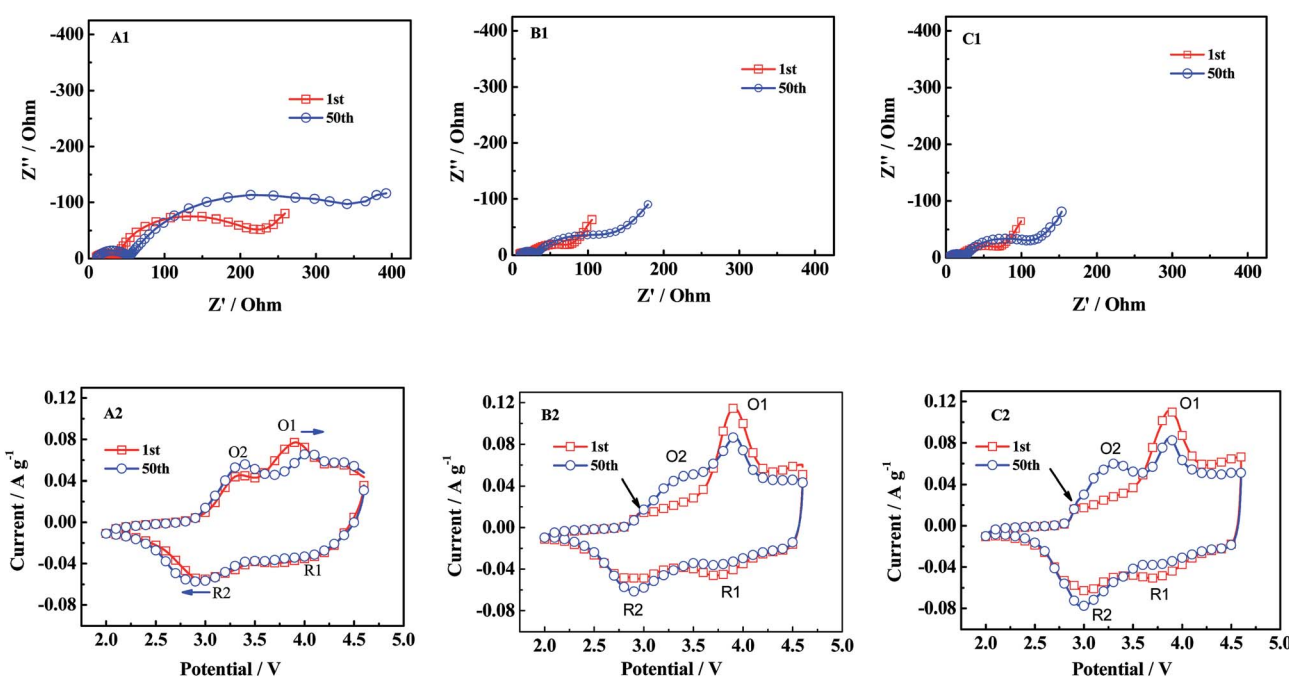


Fig. 7 Electrochemical analysis of the cells during charge/discharge cycling at the first and fiftieth cycle. Nyquist plots of LNCMO (A1), LNCMO@ Li_3PO_4 (B1) and LNCMO@ $\text{Li}_3\text{PO}_4/\text{C}$ (C1) electrodes at 4.3 V, and cyclic voltammograms of LNCMO (A2), LNCMO@ Li_3PO_4 (B2) and LNCMO@ $\text{Li}_3\text{PO}_4/\text{C}$ (C2) electrodes at a scan rate of 0.1 mV s^{-1} .

changes of the redox potentials for the LNCMO@Li₃PO₄ and LNCMO@Li₃PO₄/C electrodes are observed. In addition, the peak intensities for the oxidation and reduction of Ni and Co ions remain high for the LNCMO@Li₃PO₄ and LNCMO@Li₃PO₄/C electrodes, indicating that the mixing of the transition metal ions is suppressed during cycling.^{12,17} These CV results clearly explain the enhanced cycling stability of the LNCMO@Li₃PO₄ and LNCMO@Li₃PO₄/C materials as a result of the nanocomposite coating of Li₃PO₄ and carbon.

Conclusions

In summary, we have designed and facilely prepared the lithium-rich layered oxide Li_{1.2}Ni_{0.13}Co_{0.13}Mn_{0.54}O₂ coated with the Li₃PO₄/C composite layer (LNCMO@Li₃PO₄/C) as the cathode material for lithium ion batteries. The Li₃PO₄/C nanocomposite coating layer not only has high Li⁺ and electron mixed conductivity to improve the rate capability, but also is able to stabilize the interface between the cathode and the electrolyte to enhance the cyclability of the LNCMO@Li₃PO₄/C material. At the same time, the presence of the spinel phase, induced by the coating processes, is beneficial to suppressing the irreversible capacity loss, in addition to promoting the rate capability and cyclability. As a consequence, the LNCMO@Li₃PO₄/C cathode material exhibits an outstanding initial coulombic efficiency, high reversible capacity, excellent cyclability and desirable rate capability. Our LNCMO@Li₃PO₄/C material and the design concept provide an effective strategy for developing advanced cathode materials for lithium ion batteries, which can also be extended to other high-performance electrochemical devices.

Acknowledgements

This work was financially supported by the National High Technology Research and Development Program of China (863 Program) under Contract no. 2012AA110203.

Notes and references

- 1 M. M. Thackeray, C. Wolverton and E. D. Isaacs, *Energy Environ. Sci.*, 2012, **5**, 7854.
- 2 Y.-K. Sun, S.-T. Myung, B.-C. Park, J. Prakash, I. Belharouak and K. Amine, *Nat. Mater.*, 2009, **8**, 320.
- 3 A. S. Arico, P. Bruce, B. Scrosati, J. M. Tarascon and W. V. Schalkwijk, *Nat. Mater.*, 2005, **4**, 366.
- 4 B. Dunn, H. Kamath and J.-M. Tarascon, *Science*, 2011, **334**, 928.
- 5 G. Z. Wei, X. Lu, F. S. Ke, L. Huang, J. T. Li, Z. X. Wang, Z. Y. Zhou and S. G. Sun, *Adv. Mater.*, 2010, **22**, 4364.
- 6 J. L. Liu, L. Chen, M. Y. Hou, F. Wang, R. C. Che and Y. Y. Xia, *J. Mater. Chem.*, 2012, **22**, 25380.
- 7 J. R. Croy, S.-H. Kang, M. Balasubramanian and M. M. Thackeray, *Electrochem. Commun.*, 2011, **13**, 1063.
- 8 C. S. Johnson, N. Li, C. Lefief, J. T. Vaught and M. M. Thackeray, *Chem. Mater.*, 2008, **20**, 6095.
- 9 J. Gao and A. Manthiram, *J. Power Sources*, 2009, **191**, 644.
- 10 K. A. Jarvis, Z. Deng, L. F. Allard, A. Manthiram and P. J. Ferreira, *Chem. Mater.*, 2011, **23**, 3614.
- 11 N. Yabuuchi, K. Yoshii, S. T. Myung, I. Nakai and S. Komaba, *J. Am. Chem. Soc.*, 2011, **133**, 4404.
- 12 M. M. Thackeray, S.-H. Kang, C. S. Johnson, J. T. Vaught and R. Benedek and S. A. Hackney, *J. Mater. Chem.*, 2007, **17**, 3112.
- 13 X. Li, M. Xu, Y. Chen and B. L. Lucht, *J. Power Sources*, 2014, **248**, 1077.
- 14 M. N. Ates, Q. Jia, A. Shah, A. Busnaina, S. Mukerjee and K. M. Abraham, *J. Electrochem. Soc.*, 2014, **161**, A290.
- 15 D. Wang, I. Belharouak, X. Zhang, Y. Ren, G. Meng and C. Wang, *J. Electrochem. Soc.*, 2014, **161**, A1.
- 16 J. Liu, J. Liu, R. Wang and Y. Xia, *J. Electrochem. Soc.*, 2014, **161**, A160.
- 17 H. Yu and H. Zhou, *J. Phys. Chem. Lett.*, 2013, **4**, 1268.
- 18 H. Yu, Y. Wang, D. Asakura, E. Hosono, T. Zhang and H. Zhou, *RSC Adv.*, 2012, **2**, 8797.
- 19 A. R. Armstrong, M. Holzapfel, P. Novak, C. S. Johnson, S. H. Kang, M. M. Thackeray and P. G. Bruce, *J. Am. Chem. Soc.*, 2006, **128**, 8694.
- 20 D. Shin, C. Wolverton, J. R. Croy, M. Balasubramanian, S.-H. Kang, C. M. Lopez Rivera and M. M. Thackeray, *J. Electrochem. Soc.*, 2012, **159**, A121.
- 21 Z. Wang, E. Liu, C. He, C. Shi, J. Li and N. Zhao, *J. Power Sources*, 2013, **236**, 25.
- 22 Q. Y. Wang, J. Liu, A. Vadivel Murugan and A. Manthiram, *J. Mater. Chem.*, 2009, **19**, 4965.
- 23 Y.-K. Sun, M.-J. Lee, C. S. Yoon, J. Hassoun, K. Amine and B. Scrosati, *Adv. Mater.*, 2012, **24**, 1192.
- 24 Y. Wu and A. Manthiram, *Solid State Ionics*, 2009, **180**, 50.
- 25 J. Liu and A. Manthiram, *J. Mater. Chem.*, 2010, **20**, 3961.
- 26 G. Singh, R. Thomas, A. Kumar, R. S. Katiyar and A. Manivannan, *J. Electrochem. Soc.*, 2012, **159**, A470.
- 27 W. C. West, J. Soler and B. V. Ratnakumar, *J. Power Sources*, 2012, **204**, 200.
- 28 S. W. Cho, G. O. Kim and K. S. Ryu, *Solid State Ionics*, 2012, **206**, 84.
- 29 B. Kang and G. Ceder, *Nature*, 2009, **458**, 190.
- 30 S.-H. Wu, J.-J. Shiu and J.-Y. Lin, *J. Power Sources*, 2011, **196**, 6676.
- 31 Y. Jin, N. Li, C. H. Chen and S. Q. Wei, *Electrochem. Solid-State Lett.*, 2006, **9**, A273.
- 32 Y.-T. Cui, N. Xu, L.-Q. Kou, M.-T. Wu and L. Chen, *J. Power Sources*, 2014, **249**, 42.
- 33 H. G. Song, J. Y. Kim, K. T. Kim and Y. J. Park, *J. Power Sources*, 2011, **196**, 6847.
- 34 X. Wu, S. Wang, X. Lin, G. Zhong, Z. Gong and Y. Yang, *J. Mater. Chem. A*, 2014, **2**, 1006.
- 35 C. Deng, S. Zhang, G. S. Zhao, Z. Dong, Y. Shang, Y. X. Wu and B. D. Zhao, *J. Electrochem. Soc.*, 2013, **160**, A1457.
- 36 G. Tan, F. Wu, L. Li, R. Chen and S. Chen, *J. Phys. Chem. C*, 2013, **117**, 6013.
- 37 H. Li and H. Zhou, *Chem. Commun.*, 2012, **48**, 1201.
- 38 X. Zhou, F. Wang, Y. Zhu and Z. Liu, *J. Mater. Chem.*, 2011, **21**, 3353.

- 39 X.-L. Wu, Y.-G. Guo, J. Su, J.-W. Xiong, Y.-L. Zhang and L.-J. Wan, *Adv. Energy Mater.*, 2013, **3**, 1155.
- 40 F. Yu, J. Zhang, Y. Yang and G. Song, *J. Power Sources*, 2010, **195**, 6873.
- 41 S. Lee, Y. Cho, H.-K. Song, K. T. Lee and J. Cho, *Angew. Chem., Int. Ed.*, 2012, **51**, 8748.
- 42 B. Lin, Z. Wen, X. Wang and Y. Liu, *J. Solid State Electrochem.*, 2010, **14**, 1807.
- 43 H. Liu, C. Du, G. Yin, B. Song, P. Zuo, X. Cheng, Y. Ma and Y. Gao, *J. Mater. Chem. A*, 2014, **2**, 15640.
- 44 F. Yu, S. Ge, B. Li, G. Sun, R. Mei and L. Zheng, *Curr. Inorg. Chem.*, 2012, **2**, 194.
- 45 S. Zhao, H. Ding, Y. Wang, B. Li and C. Nan, *J. Alloys Compd.*, 2013, **566**, 206.
- 46 Q. Y. Wang, J. Liu, A. Vadivel Murugan and A. Manthiram, *J. Mater. Chem.*, 2009, **19**, 4965.
- 47 J.-H. Park, J.-M. Kim, C. K. Lee and S.-Y. Lee, *J. Power Sources*, 2014, **263**, 209.
- 48 S.-H. Park, S.-W. Oh, C.-S. Yoon, S.-T. Myung and Y.-K. Sun, *Electrochem. Solid-State Lett.*, 2005, **8**, A163.